During hippocampal inactivation, grid cells maintain their synchrony, even when the grid pattern is lost

Noam Almog[1], Gilad Tocker[1,2ξ], Tora Bonnevie[3∞], Edvard Moser[3], May-Britt Moser[3] and Dori Derdikman[1‡]

[1]*Rappaport Faculty of Medicine and Research Institute, Technion – Israel Institute of Technology.*

[2]*Gonda Multidisciplinary Brain Research Center, Bar Ilan University.*

[3]*Kavli Institute for Systems Neuroscience and Centre for Neural Computation, Norwegian University of Science and Technology.*

‡Corresponding author. Email: derdik@technion.ac.il

ξ *Present address: Department of Neurobiology, Northwestern University, Evanston, Illinois.*

∞ *Present address: Department of Neuromedicine and Movement Science, Norwegian University of Science and Technology.*

Abstract

The grid cell network in the MEC has been subject to thorough testing and analysis, and many theories for their formation have been suggested. To test some of these theories we re-analyzed data from Bonnevie et al. (2013), in which the hippocampus was inactivated and grid cells were recorded in the MEC, to investigate whether the firing associations of grid cells depend on hippocampal inputs. Specifically, we examined temporal and spatial correlations in the firing times of simultaneously recorded grid cells before and during hippocampal inactivation. Our analysis revealed evidence of network coherence in grid cells even in the absence of hippocampal input to the MEC, both in regular grid cells and in those that became head-direction cells after hippocampal inactivation. This favors models which suggest that phase relations between grid cells in the MEC are dependent on intrinsic connectivity within the MEC.

Introduction

the grid cell mechanism is arguably one of the best-tested and best established mechanisms, across neural circuits in the mammalian CNS, thanks to extensive testing and analysis (Hafting et al., 2005,

Moser et al., 2008, Derdikman, D., & Knierim, J. J., 2014, Rowland et al., 2016). Modeling work has suggested that either grid cells are generated intrinsically in the MEC, for example by a continuous attractor network model (Burak & Fiete, 2009; Couey et al., 2013; Fuhs & Touretzky, 2006; Giocomo, Moser, & Moser, 2011; Moser, Moser, & Roudi, 2014; Zilli, 2012) or alternatively have their properties form through an interaction with another region, such as the hippocampus (Dordek, Soudry, Meir, & Derdikman, 2016; Kropff & Treves, 2008; Stachenfeld, Botvinick, & Gershman, 2017). To dissociate between these possibilities, we re-analyzed data from Bonnevie et al. (2013), who inactivated hippocampal input to the MEC, and found that under this condition, the grid pattern of individual grid cells deteriorated significantly or disappeared entirely. Here we investigated whether the firing associations of grid cells depend on hippocampal inputs. Specifically, we examined correlations in the firing times of simultaneously recorded grid cells before and during hippocampal inactivation, including grid cells that acquired head directional tuning during inactivation. Our analysis yielded evidence of network coherence in grid cells even in the absence of hippocampal input to the MEC.

Results

We reanalyzed data from Bonnevie et al. (2013) in which grid cells were recorded before, during and after hippocampal inactivation (Figure 1A-C). A total of 301 well-separated cells were recorded in the MEC and parasubiculum across 40 sessions including pre-, during and post-hippocampal inactivation, with 2-18 cells recorded simultaneously per session. While the runs of pre- and post-inactivation were analyzed in their entirety, for runs during inactivation we used only the time period starting at 15 minutes or later, up to 45 minutes, during which the most data were available across all recordings. The analysis showed similar effects on grid behavior in longer trials as in the first 45 minutes; the average grid score was -0.063±0.193 for the first 15-45 minutes and -0.051±0.180 for the remainder minutes.

We searched for evidence of network activity between grid cells in the absence of hippocampal input. Consequently, we examined spike time correlations and spatial firing correlations between simultaneously recorded cells whose gridness were high under normal conditions, but deteriorated during hippocampal inactivation (Figure 1D, 1E). To select only cells with significant gridness before inactivation and minimal gridness during inactivation, we used a minimum grid score threshold of 0.5 pre inactivation, and maximum of 0.2 during inactivation. Doing the same analysis with different thresholds, ranging from 0.2 to 0.9 pre inactivation, and 0 to 0.4 during inactivation, did not change the central finding of the analysis, showing persistence of temporal correlations between cell pairs during the inactivation (Figure 3 figure supplement 5).

The mean grid score of the selected cells was 0.92±0.24 pre-inactivation and -0.30±0.24 during inactivation. Additionally, to ensure that the same cell was not recorded on different electrodes, we removed any cells from a single recording session whose individual spike times overlapped within a 1 ms window more than 5% of the time (this mostly removed cases with very large overlap that were suspected as originating from the same cell on different tetrodes). The mean spike overlap after exclusion was 0.57%±0.65 of the total spike strain. In total, 45 of 301 cells from 17 of 41 recording sessions met our criteria (Figure 1D), producing 107 pairs of simultaneously recorded cells, on which the results of this study are based. In our cohort, firing rates decreased by 50.0% during inactivation, and returned to 90.5% of original levels post-inactivation (pre 1.1Hz±0.90, during 2.00Hz±1.16, and post 2.00Hz±1.16). However, overall, neither the firing rate, nor the grid score seemed to correlate to temporal or spatial correlations both pre and during inactivation (Figs. 1B, 1C, 1E; Figure 4 figure supplement 1).

Temporal correlations are maintained during loss of gridness

We found that several simultaneously recorded grid cell pairs consistently maintained temporal correlations even as their gridness deteriorated (Figure 2A, 2B). Compared to random shuffling (n=1000, α=0.01), these correlations were statistically significant; 57%, 26%, and 53% of correlations passed the shuffling significance test pre-, during, and post-inactivation, respectively. Of the statistically significant correlations, 41%, 8%, and 27% were negative for the three respective recording phases, while 16%, 19%, and 22% were positive. Temporal correlations pre- vs. during inactivation were correlated at r=0.57 (Figure 3A, P<0.001; although the distributions were different, Wilcoxon signed-rank P<0.001), and pre- vs. post-inactivation were correlated at r=0.86 (Figure 3A, P<0.001). The results were very similar when analyzing the period of the recordings after 45 minutes (Figure 3 figure supplement 1). The strength of the correlation both before and during inactivation demonstrated a slight non-significant positive dependence on the grid score (Figure 3 figure supplement 2). For comparison, the correlation coefficient of temporal correlations pre- vs. during for each cell from our cohort against each cell not from the same recording session (1854 pairs total) was r = -0.03 (P=0.21).

Spatial correlations are maintained during loss of gridness

To examine whether short-range spatial correlations were maintained also during hippocampal inactivation, we employed a similar method, which compared the correlation coefficient of the 2D firing rate maps at the same position (x,y = 0,0). Overall, spatial correlations did not persist as consistently as temporal correlations during hippocampal inactivation; however, some degree of persistence was

present between simultaneously recorded cell pairs. Spatial correlations were correlated to each other pre-inactivation vs. during inactivation at r=0.34 (Figure 3C, P<0.001), while pre- vs. post-spatial correlations were correlated at r=0.88 (Figure 3C, P<0.001). For a control comparison, the correlation coefficient of spatial correlations pre- vs. during inactivation for each cell from our cohort correlated against each other cell not from the same recording session, was lower (r = 0.10, P<0.001). The shuffling significance test (n=1000, α=0.01) found that 30%, 7%, and 22% of spatial correlations were significant pre-, during, and post- inactivation, respectively. Of the correlations, 18%, 1%, and 6% were negatively significant for all three recording phases, respectively, while 12%, 6%, and 13% were positive (Figure 3B,D). We note though that the amount of cell pairs was significantly lower during inactivation ($\chi 2$=12.2, P<0.001). The angular direction of the nearest peak in the spatial correlations was not maintained (Figure 3 figure supplement 6: while "pre" vs. "post" difference in angle was very non-uniform (Rayleigh non-uniformity test, P<0.001), the difference in angle between "pre" and "during" did not diverge from uniformity (Rayleigh non-uniformity test, P=0.974), however when performing a time-windowed analysis of spatial correlations (see Methods), at least in the 1-second range there were comparable correlations between spatial patterns before and during inactivation to those after inactivation (Figure 3 figure supplement 4). Although the statistical significance was lower overall for spatial correlations than for temporal correlations, the results for spatial correlations were consistent with those for temporal correlations. Additionally, plotting temporal and spatial correlations against each other demonstrated a clear linear relationship; the correlations of temporal to spatial correlations were r = 0.90 (P<0.001), r = 0.72 (P<0.001), and r = 0.90 (P<0.001) for pre-, during, and post- inactivation, respectively (Figure 3 figure supplement 3).

Temporal correlations but not spatial correlations persisted during inactivation for grid-turned-head directional cells

In the original Bonnevie et al. (2013) study, it was reported that a subset of grid cells became head direction cells during hippocampal inactivation. Cells within our cohort showed a bi-modal distribution of Rayleigh head-direction tuning scores during inactivation (Figure 4C). This enabled selecting the cells that became head-direction cells, defined as having a Rayleigh score smaller than 0.4 pre, and greater than 0.4 during inactivation (15 of the 63 cells in our cohort, from 3 of the 17 recording sessions in two rats; 46 pairs out of the 107 pairs) and those which did not, defined as staying below 0.4 both pre and during inactivation (39 of the 63 cells in our cohort, from 13 of the 17 recording sessions in six rats; 46 pairs out of the 107 pairs) (Figures 4C, D and E). Figure 4A depicts an example of these grid-turned head direction cells from the same recording session. Examining these two clusters separately, looking at

temporal correlations pre- and during inactivation, non-head direction pairs were more correlated at r=0.71, than the head direction pairs at r=0.52, though both were correlations were significant $p<0.01$ (Figure 4D). For spatial correlations, pre-inactivation compared to during inactivation, had a correlation coefficient of r=0.46 $p<0.01$ in the non-head directional cluster, and r=0.22 in the head direction cluster, though this latter correlation was not significant with p=0.19 (Figure 4D). In conclusion, while spatial correlations were probably less persistent in grid-turned head direction cells, temporal correlations persisted similarly in both, regular and grid-turned-head direction cells during hippocampal inactivation. There did seem to be a bias in the tuning angle for the grid turned head direction cells whose average was 37.0°±3.5 during inactivation, which was also seen in the rest of the cells in the population, whose Rayleigh Score was also above the same threshold of 0.4 pre and during inactivation. Their averages were 26.5°±6.1, and 38.7°±4.5 respectively (Figure 4E, 4F). This bias is consistent with the fact that all the grid-turned head direction cells were recorded in the same room (room 3), as were the majority of the rest of the cells (Figure 4 figure supplement 2).

Discussion

This study reanalyzed data from Bonnevie et al. (2013), in which hippocampal input to the MEC was inactivated. The aim was to examine possible evidence of local grid cell coordination. We found that despite the disappearance of the grid pattern of these cells during hippocampal inactivation, temporal correlations between grid cells remained, as did local spatial correlations, although to a lesser, yet still statistically significant degree. A time-windowed version of the spatial correlations suggests a window of about 1-second in which spatial structure remained.

First, these findings assert that hippocampal input does not account for spatially and temporally correlated activity between grid cells. Second, the slow decay of the correlations at a timescale in the order of magnitude of 1 second indicates that this effect is not due solely to direct synaptic connectivity, but to recurrent network activity of dense networks in behavioral timescales. Last, some grid cells became head-direction cells during hippocampal inactivation, and their spatial correlations were less dominant; nonetheless, temporal correlations persisted equally. Taken together, this paper is adding another piece of evidence to a line of results that support continuous attractor dynamics (Burak & Fiete, 2009; Couey, et al., 2013; Fuhs & Touretzky, 2006; Giocomo, et al., 2011; Moser, et al., 2014; Zilli, 2012, Yoonet al., 2013, Heys et al., 2015, Gu et al., 2018, Trettel et al. 2019, Gardner et al., 2019) while being less supportive of feedforward models creating grid cells through summation of information from the hippocampus (Dordek, et al., 2016; Kropff & Treves, 2008; Stachenfeld, et al., 2017). We cannot

preclude, though, the possibility that grid cells are formed through a different feedforward process, not involving the hippocampus, or that they are generated through a recurrent loop involving information from both the hippocampus and the entorhinal cortex (Donato, Jacobsen, Moser, & Moser, 2017).

A network model for grid cell firing pattern at least strongly predicts, if not implicitly requires, a significant level of synchronicity in temporal firing between two networked grid cells (Moser, et al., 2014). The attractor manifold model for grid pattern generation predicts that even when the network is deprived of spatial input, in this case from the hippocampus, the activity pattern that is maintained (though no longer anchored to physical space) would cause nearby cells in the manifold to fire with high correlation, and more distant cells not to fire (Burak & Fiete, 2009; Dunn, Mørreaunet, & Roudi, 2014; Fuhs & Touretzky, 2006; Tocker, Barak, & Derdikman, 2015). This aligns with our observations of both correlated and anticorrelated activity during inactivation.

In addition to the evidence of network coordination, we found that the distinct subset of cells that became head direction-tuned during inactivation, maintained temporal but not spatial correlations during hippocampal inactivation. Interestingly, the head-direction selectivity of these cells was very biased (Fig. 4E), consistent with the observation of the remaining temporal correlations. This subset of grid-turned-head-direction cells is likely defined by strong input from the retrosplenial cortex, or the pre- or para- subiculum, which also project into the MEC, and which dominate these cells' spatial tuning and firing time synchronization in the absence of input from the hippocampus (Clark & Taube, 2012). Because the conjunctive grid-head direction cells originated from recordings that did not contain pure grid cells, we did not observe direct evidence of a temporal correlation between grid cells that became head-direction cells and those that did not. Notably, both groups were similar in their temporal correlation values before and during inactivation, regardless of their differences in spatial correlations. This suggests that despite receiving additional spatial input, the grid cells that became head-direction cells were part of the grid-cell network.

Several other experiments have investigated grid cell activity when spatial input was curtailed, specifically following removal of visual input. In their original paper that described grid cells, Hafting et al. (2005) observed rat grid cells in darkness, and found that the grid pattern did not deteriorate. More recently, two studies, by Perez-Escobar et al. (2016) and Chen et al. (2016) that examined mouse grid cells in darkness reported that the grid pattern deteriorated without visual input. Furthermore, both studies found that significant temporal correlations were maintained during impaired spatial input to

166 the entorhinal cortex, in accordance with our findings. Similarly, two new studies have demonstrated
167 that grid cell temporal correlations remain during sleep (Trettel et al., 2019, Gardner, et al., 2019).

168 The steady synchronicity in our study suggests an underlying network structure in the MEC that is
169 responsible for grid cell formation. This corroborates the idea of an attractor manifold involved in grid
170 cell formation.

Methods

171 The following sections describe the acquisition of the original data from Bonnevie et al. (2013), and the
172 analytical methods we applied to the data. All code was written in MATLAB (V. 2018b). The code was
173 uploaded to GitHub at github.com/noamza/muscimol.

174 Input data

175 Briefly, the original experiment by Bonnevie et al. (2013) was performed with 8 male, 3-5 month old
176 Long-Evans rats, with water available *ad libitum*. The rats were kept on a 12h light, 12h dark schedule
177 and tested in the dark phase. Rats were implanted with a microdrive connected to four tetrodes of
178 twisted 17-µm platinum-iridium wire; one bundle was implanted in the MEC in all rats, anteroposterior
179 0.4–0.5 mm in front of the transverse sinus, mediolateral 4.5–4.6 mm from the midline, and
180 dorsoventral 1.4–1.8 mm below the dura. Tetrodes were angled 10° in the sagittal plane. For
181 hippocampal inactivation, cannulae were implanted at a 30° angle in the posterior direction towards the
182 dorsal hippocampus; 0.24–0.30µl of the $GABA_A$ receptor agonist muscimol (5-aminomethyl-3-
183 hydroxyisoxazole) diluted in PBS was used to inactivate the hippocampus.

184 Rats were run in an open-field 100cm, 150cm, or 170cm square arena, size depending on which of 3
185 recording rooms were used, polarized by a single white que card in an otherwise black environment for
186 a 20 min period, after which muscimol was infused. Subsequently, the firing rate of all principal cells
187 recorded in the dorsal CA1 region decreased rapidly, ~2.2 mm posterior and lateral to the infusion site
188 (82 cells, all of which were place cells), with firing rates dropping to 1% of the baseline rate in 79% of the
189 recorded cells within 20 minutes. Inactivation of the hippocampus had only minimal impact on the
190 behavior of the rats. Rats then ran for an average of 160 minutes in the open field. After 6-24 hours, the
191 rats were run for 20 minutes to check for cell recovery and grid stability.

192 Quantifying gridness and head direction selectivity

193 For this analysis, we were interested in specifically examining grid cells whose spatial firing pattern was
194 significantly degraded. To quantify this, we used the generally accepted measure of grid score, which

essentially measures the extent the cell's firing pattern repeats itself at 60° intervals on a two-dimensional (2D) plane (how hexagonal the firing pattern is). The procedure undertaken to achieve this calculation is as follows (based on the procedure described in (Sargolini et al., 2006; Tocker, et al., 2015)):

The arenas were divided into 2500 equally sized square bins. First, a 2D map of neuron spiking was generated by creating a matrix where the index [i, j] represents the location in the arena, and the value represents the number of spikes in that location. The equivalent matrix for time spent at each location was also created. These two matrixes were divided by each other element-wise, creating a matrix of firing rates at each location bin.

Next, a 2D normalized spatial autocorrelation was performed on the rate map matrix accounting for non-existent values in the rate map, as described in Tocker, et al., 2015. Firing fields were identified using a method that treated the smoothed (2D Gaussian smoothing with σ=2) autocorrelation matrix as an image, and identified distinct regions bounded by a given pixel value of *x* in all 8 directions whose external values are all less than *x*. Typical grid cell autocorrelations have at least 6 firing fields, at approximately 60° intervals (Hafting, et al., 2005). Cells whose autocorrelation did not create 6 distinct firing fields for calculating the anulus using the above method were set to a default grid score of 0. Typical grid cell activity was manifested as equidistant firing fields at 60° intervals from each other.

The final step in calculating the grid score was to create a ring around the center of the smoothed autocorrelation (2D Gaussian smoothing with σ=2), with an inner radius small enough to contain the innermost firing field, and the outer radius large enough to contain the outermost edge of the sixth closest field. Next, the ring was rotated 60° and correlated to the original (using a normalized correlation, accounting for empty matrix values as described above). This value was then subtracted by the value of the ring correlated at a 30° rotation. Since both correlations have values in the range of [-1,1], the range of grid scores is [-2, 2].

A Rayleigh score from 0 to 1 was used to quantify head directionality of cells, similar to that described in Tocker et al. (2015).

Cell pair correlations

To quantify temporal correlations between cells, we calculated the Pearson correlation of their spike trains (lag = 0ms). For spatial correlations, a 2D Pearson correlation of the rate maps (see Quantifying Gridness) was performed and compared at [0,0]. Spatial cross correlations were done following the

Pearson moment formula accounting for missing values in the rate map as described in Tocker, et al., 2015. Smoothing was done on the spike trains prior to both temporal and spatial correlations using a moving average window of 25ms. Smoothing windows from 1ms to 1000ms had little or no impact on the correlation results.

Shuffling to measure significance

To measure the statistical significance of the correlations, we employed a shuffling method in which spike trains were randomly shifted cyclically n times (n=1000 unless stated otherwise) and their correlations recalculated. Correlations were considered significant if they were in the 99th percentile when compared to the shuffled correlations.

Time-windowed spatial correlation analysis

In order to measure spatial correlations at a smaller time-scale during inactivation, we analyzed spike to spike locations relative to the first cell in a cell pair within a given time window. For a given cell pair, each spike was treated as the origin in two dimensional space [0,0], and a 2D binned rate map (see above) consisting of all spikes in a given time window [± 1s 2s 3s 5s or 10s], was constructed. This collection of rate maps for a given cell pair was aggregated into a single rate map by adding up the values at a given bin location in the rate map. This procedure was done for each recording session [pre during post]. These cell pair maps were then spatially correlated against each other by session [pre vs during, pre vs post], where [pre vs post] represented the control in which we expected to see stable maps for cell pairs between pre and post and therefore high correlations.

Acknowledgements

We thank Cindy Cohen for proofreading. We thank Chen Elbak and Irina Reiter for help with experiment administration. We thank members of the Derdikman lab for fruitful discussions.

Funding

The research was supported by the Israel Science Foundation personal grants #955/13, #2344/16 and #2655/18, by the German-Israeli Foundation for Scientific Research and Development, by a Rappaport Institute grant, by the Allen and Jewel Prince Center for Neurodegenerative Disorders of the Brain grant, and by a joint Technion-Weizmann Adelis foundation grant.

Conflict of Interest Statement

The authors declare that the research was conducted in the absence of any commercial or financial relationships that could be construed as a potential conflict of interest.

References

Bonnevie, T., Dunn, B., Fyhn, M., Hafting, T., Derdikman, D., Kubie, J. L., . . . Moser, M.-B. (2013). Grid cells require excitatory drive from the hippocampus. *Nature Neuroscience, 16*(3), 309-317.

Moser, E. I., Kropff, E., & Moser, M. B. (2008). Place cells, grid cells, and the brain's spatial representation system. Annu. Rev. Neurosci., 31, 69-89

Derdikman, D., & Knierim, J. J. (Eds.). (2014). Space, time and memory in the hippocampal formation. Vienna: Springer Vienna

Rowland, D. C., Roudi, Y., Moser, M. B., & Moser, E. I. (2016). Ten years of grid cells. Annual review of neuroscience, 39, 19-40

Burak, Y., & Fiete, I. R. (2009). Accurate path integration in continuous attractor network models of grid cells. *PLoS computational biology, 5*(2), e1000291.

Chen, G., Manson, D., Cacucci, F., & Wills, T. J. (2016). Absence of visual input results in the disruption of grid cell firing in the mouse. *Current Biology, 26*(17), 2335-2342.

Clark, B. J., & Taube, J. S. (2012). Vestibular and Attractor Network Basis of the Head Direction Cell Signal in Subcortical Circuits. [Review]. *Frontiers in Neural Circuits, 6*. doi: 10.3389/fncir.2012.00007

Couey, J. J., Witoelar, A., Zhang, S.-J., Zheng, K., Ye, J., Dunn, B., . . . Witter, M. P. (2013). Recurrent inhibitory circuitry as a mechanism for grid formation. [10.1038/nn.3310]. *Nat Neurosci, 16*(3), 318-324. doi: http://www.nature.com/neuro/journal/v16/n3/abs/nn.3310.html#supplementary-information

Donato, F., Jacobsen, R. I., Moser, M.-B., & Moser, E. I. (2017). Stellate cells drive maturation of the entorhinal-hippocampal circuit. *Science, 355*(6330), eaai8178. doi: 10.1126/science.aai8178

Dordek, Y., Soudry, D., Meir, R., & Derdikman, D. (2016). Extracting grid cell characteristics from place cell inputs using non-negative principal component analysis. [JOUR]. *eLife, 5*, e10094. doi: 10.7554/eLife.10094

Dunn, B., Mørreaunet, M., & Roudi, Y. (2014). Correlations and functional connections in a population of grid cells. *arXiv preprint arXiv:1405.0044*.

Fuhs, M. C., & Touretzky, D. S. (2006). A spin glass model of path integration in rat medial entorhinal cortex. *Journal of Neuroscience, 26*(16), 4266-4276. doi: Doi 10.1523/Jneurosci.1353-05.2006

279 Giocomo, Lisa M., Moser, M.-B., & Moser, Edvard I. (2011). Computational Models of Grid Cells. *Neuron,*
280 *71*(4), 589-603.
281 Hafting, T., Fyhn, M., Molden, S., Moser, M.-B., & Moser, E. I. (2005). Microstructure of a spatial map in
282 the entorhinal cortex. *Nature, 436*(7052), 801.
283 Kropff, E., & Treves, A. (2008). The emergence of grid cells: Intelligent design or just adaptation?
284 *Hippocampus, 18*(12), 1256-1269.
285 Moser, E. I., Moser, M.-B., & Roudi, Y. (2014). Network mechanisms of grid cells. *Philosophical*
286 *Transactions of the Royal Society B: Biological Sciences, 369*(1635), 20120511.
287 Perez-Escobar, J. A., Kornienko, O., Latuske, P., Kohler, L., & Allen, K. (2016). Visual landmarks sharpen
288 grid cell metric and confer context specificity to neurons of the medial entorhinal cortex. *eLife,*
289 *5*, e16937.
290 Sargolini, F., Fyhn, M., Hafting, T., McNaughton, B. L., Witter, M. P., Moser, M. B., & Moser, E. I. (2006).
291 Conjunctive representation of position, direction, and velocity in entorhinal cortex. *Science,*
292 *312*(5774), 758-762. doi: 312/5774/758 [pii]10.1126/science.1125572

293 Stachenfeld, K. L., Botvinick, M. M., & Gershman, S. J. (2017). The hippocampus as a predictive map.
294 *Nature Neuroscience, 20*(11), 1643.
295 Tocker, G., Barak, O., & Derdikman, D. (2015). Grid cells correlation structure suggests organized
296 feedforward projections into superficial layers of the medial entorhinal cortex. *Hippocampus,*
297 *25*(12), 1599-1613. doi: 10.1002/hipo.22481
298 Zilli, E. A. (2012). Models of grid cell spatial firing published 2005-2011. [Review]. *Frontiers in Neural*
299 *Circuits, 6*. doi: 10.3389/fncir.2012.00016

300 *Yoon, K., Buice, M. A., Barry, C., Hayman, R., Burgess, N., & Fiete, I. R. (2013). Specific evidence of low-*
301 *dimensional continuous attractor dynamics in grid cells. Nature neuroscience, 16(8), 1077*
302 *Heys, J. G., Rangarajan, K. V., & Dombeck, D. A. (2014). The functional micro-organization of grid cells*
303 *revealed by cellular-resolution imaging. Neuron, 84(5), 1079-1090*
304 *Dunn, B., Mørreaunet, M., & Roudi, Y. (2015). Correlations and functional connections in a population of*
305 *grid cells. PLoS computational biology, 11(2), e1004052*
306 *Gu, Y., Lewallen, S., Kinkhabwala, A. A., Domnisoru, C., Yoon, K., Gauthier, J. L., ... & Tank, D. W. (2018). A*
307 *map-like micro-organization of grid cells in the medial entorhinal cortex. Cell, 175(3), 736-750*

Trettel, S. G., Trimper, J. B., Hwaun, E., Fiete, I. R., & Colgin, L. L. (2019). Grid cell co-activity patterns during sleep reflect spatial overlap of grid fields during active behaviors. Nature neuroscience, 22(4), 609

Gardner, Richard J., et al. "Correlation structure of grid cells is preserved during sleep." Nature neuroscience 22.4 (2019): 598

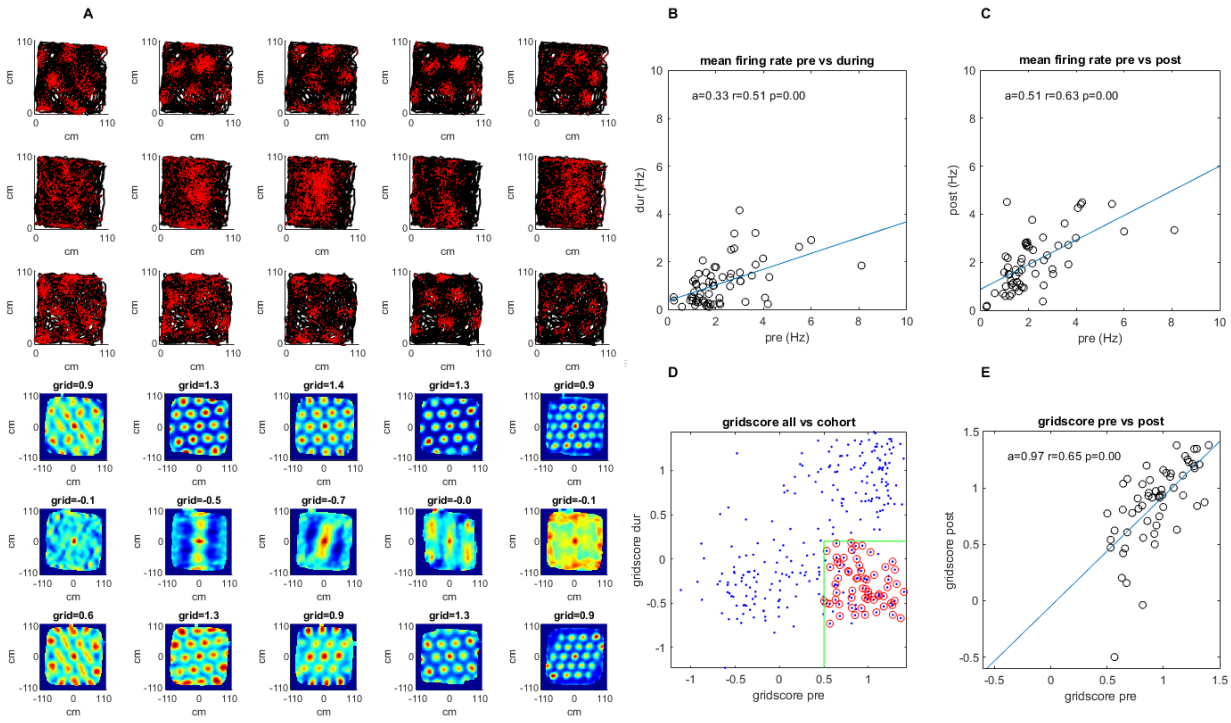

Figure 1. A survey of the grid cell population included in the study. Recordings were made pre-, during, and post-injection of muscimol to the hippocampus. (**A)** A sample group of 5 simultaneously recorded grid cells, one cell per column. The first three plots in each column show the location of a single cell firing (red) along the rat's trajectory (black) in a square arena pre-, during, and post-hippocampal inactivation, respectively. The last three plots in each column show the autocorrelation of the firing rate map (the number of times the cell fired at each location divided by the amount of time spent there by the animal) and the grid score of that session pre-, during, and post inactivation. (**B**) The mean firing rate for the 45 grid cells included in the study pre- vs. during inactivation. (**C**) Same as (B) but for pre- vs. post-inactivation. (**D**) The grid score of all cells in the dataset vs. those included in the study. Red circles show the cells from the total population that were ultimately included in the study meeting the minimum and maximum grid score threshold pre and during respectively (green), as well as the additional criteria specified in the Methods section (note that cells whose grid scores could not be calculated were set to 0). (**E**) Grid score pre- and post- inactivation of the cells included in the study.

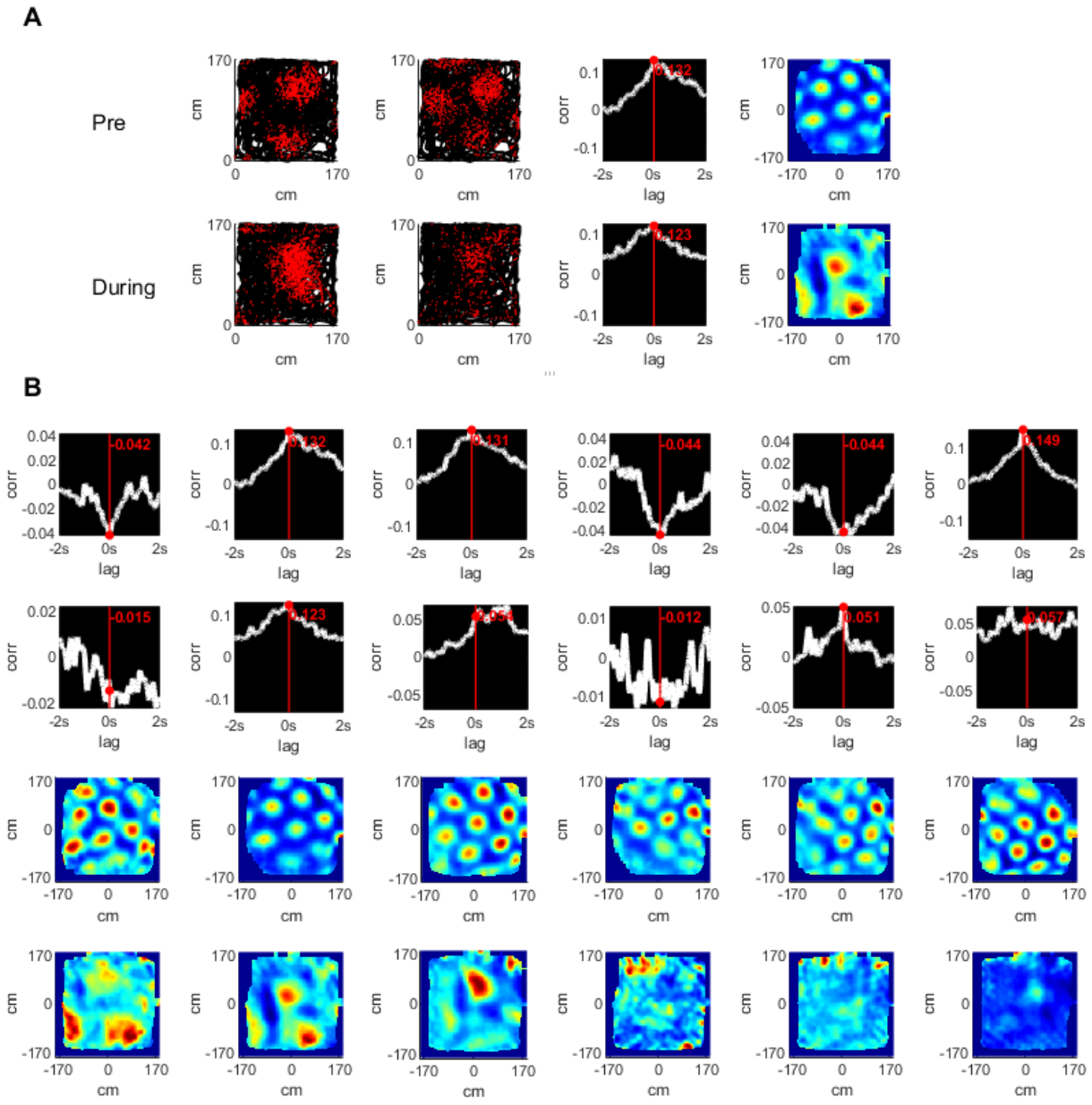

Figure 2. Temporal and spatial cross correlations of simultaneously recorded grid cells pre- and during hippocampal inactivation. (**A**) An example of a pair of simultaneously recorded grid cells (columns 1, 2); the location of the cell firing (red) plotted over the rat's trajectory (black) in a square arena. Columns 3 and 4 show the temporal and spatial cross correlation of the firing rate maps of the cells respectively. Rows show the same analysis pre- and during inactivation. (**B**) The temporal and spatial cross correlations of cell pairs of an entire group of simultaneously recorded grid cells. Rows 1, 2 show temporal correlations pre- and during inactivation; rows 3, 4 show the same for spatial cross correlations.

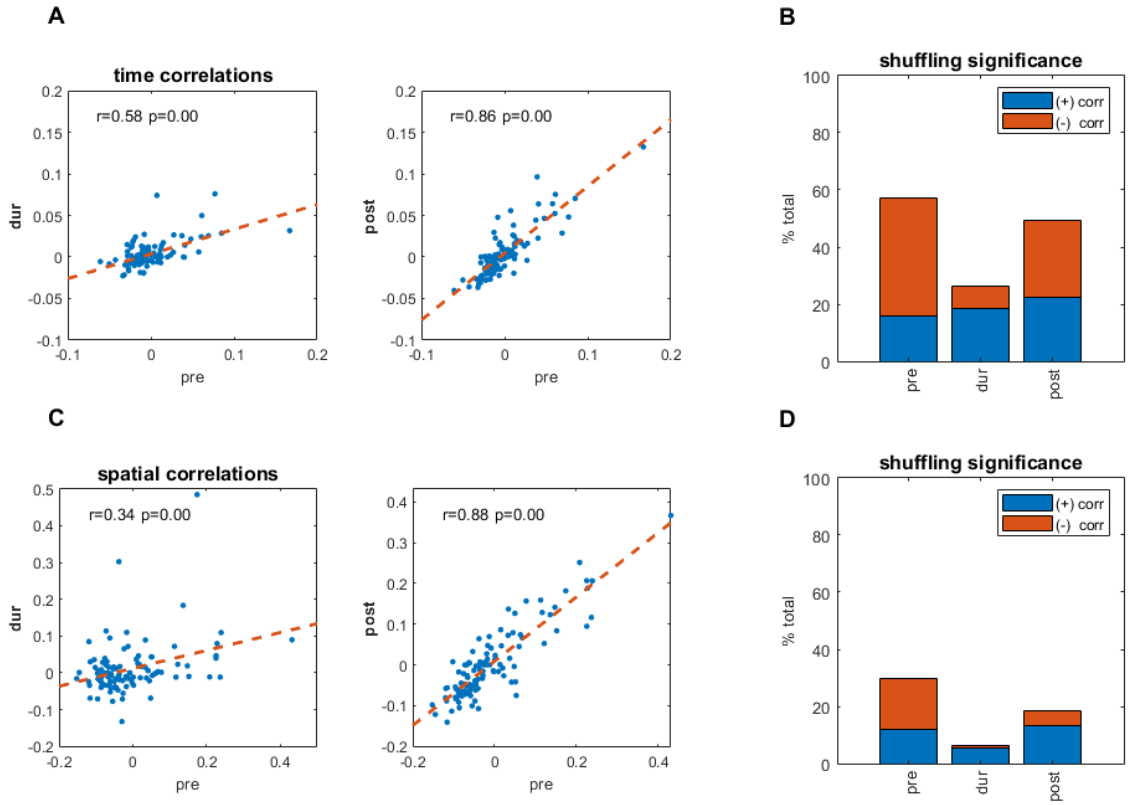

Figure 3 (with 6 supplements). Temporal and spatial correlations pre- and during inactivation. (**A**) Temporal cross correlations pre- and during inactivation, and pre- and post- inactivation, with correlation value (r), and corresponding p-value (**B**) Proportions of significant temporal correlations, according to shuffling measures, pre-, during, and post-inactivation, including the sign (positive, negative) of the correlation value. (**C**) Same as (A) but for spatial correlations of the firing pattern in the arena at [0,0]. (**D**) Same as (B) but for spatial correlations of the firing pattern in the arena at [0,0].

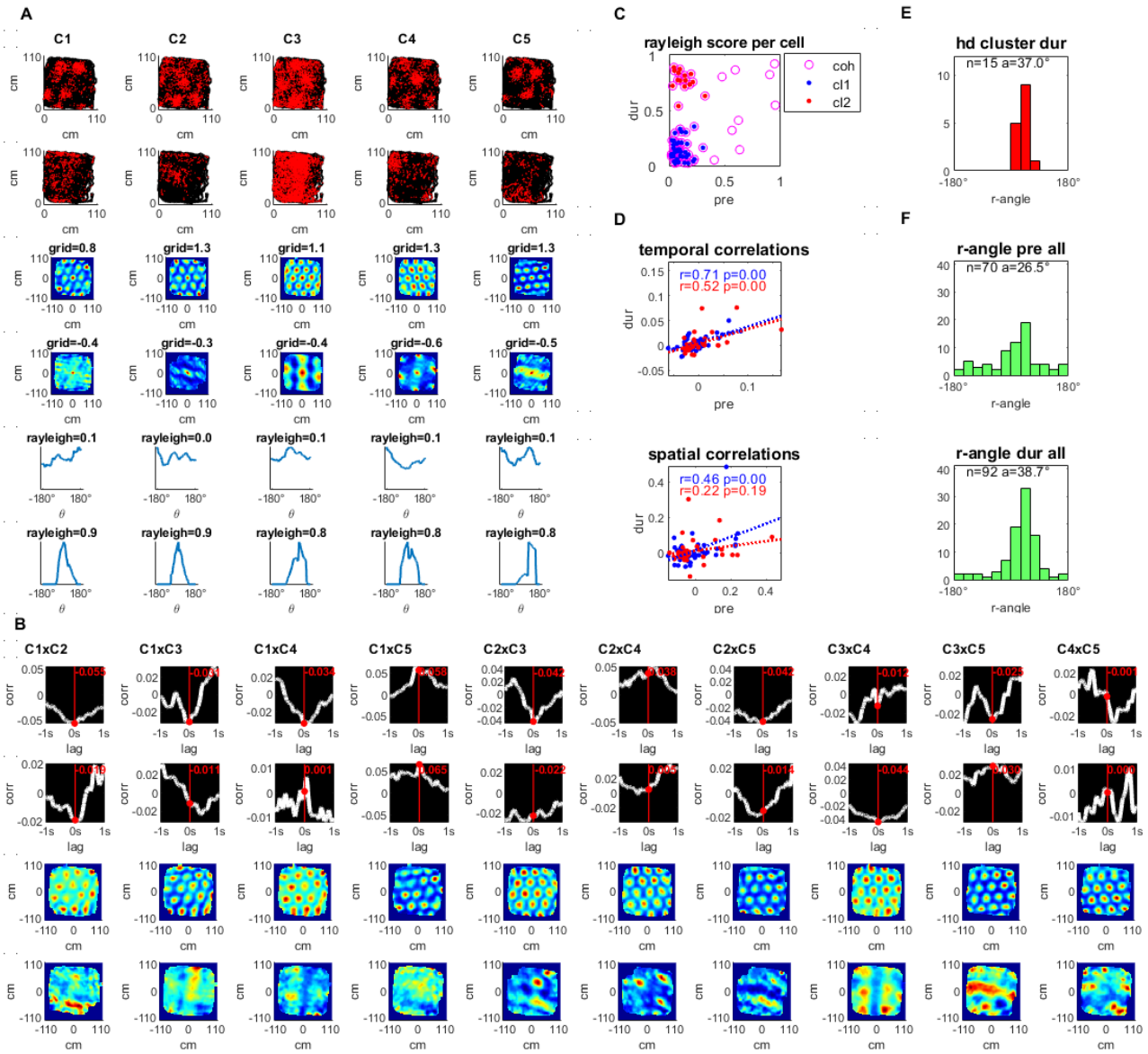

Figure 4 (with 2 supplements). Simultaneously recorded grid cells that became head directional during hippocampal inactivation. (**A**) A sample group of 5 simultaneously recorded grid cells, one cell per column. The first two plots in each column show the location of a single cell firing (red) along the rat's trajectory (black) in a square arena pre- and during hippocampal inactivation. Next, two plots show the autocorrelation of the firing rate map and the associated grid score pre- and during inactivation. The last two plots in the column show the firing rate by head direction for an associated Rayleigh Score, pre and during inactivation. (**B**) Temporal and spatial cross correlations for each cell pair of the group, pre- and during inactivation by column. (**C**) Rayleigh scores pre- and during inactivation for all cells in the cohort (magenta circles) clustered by low head directionality (Rayleigh Score < 0.4 pre- and during inactivation, blue) and high head directionality (Rayleigh Score < 0.4 pre- and > 0.4 during inactivation, red) (**D**)

Temporal and Spatial correlations (at 0,0) pre- and during inactivation grouped by head directionality clusters defined in (C), with the trendline slope (a) correlation coefficient (r), and corresponding p-value (p). (**E**) Histogram of Rayleigh angles for the cells in the HD cluster (red cluster in panels C and D) during inactivation (angles pre inactivation are not shown since these cells had low Rayleigh scores for that period). (**F**) Rayleigh Angles for all cells in population with Rayleigh Score > 0.4 pre, and during inactivation.

314

Supplement Figures

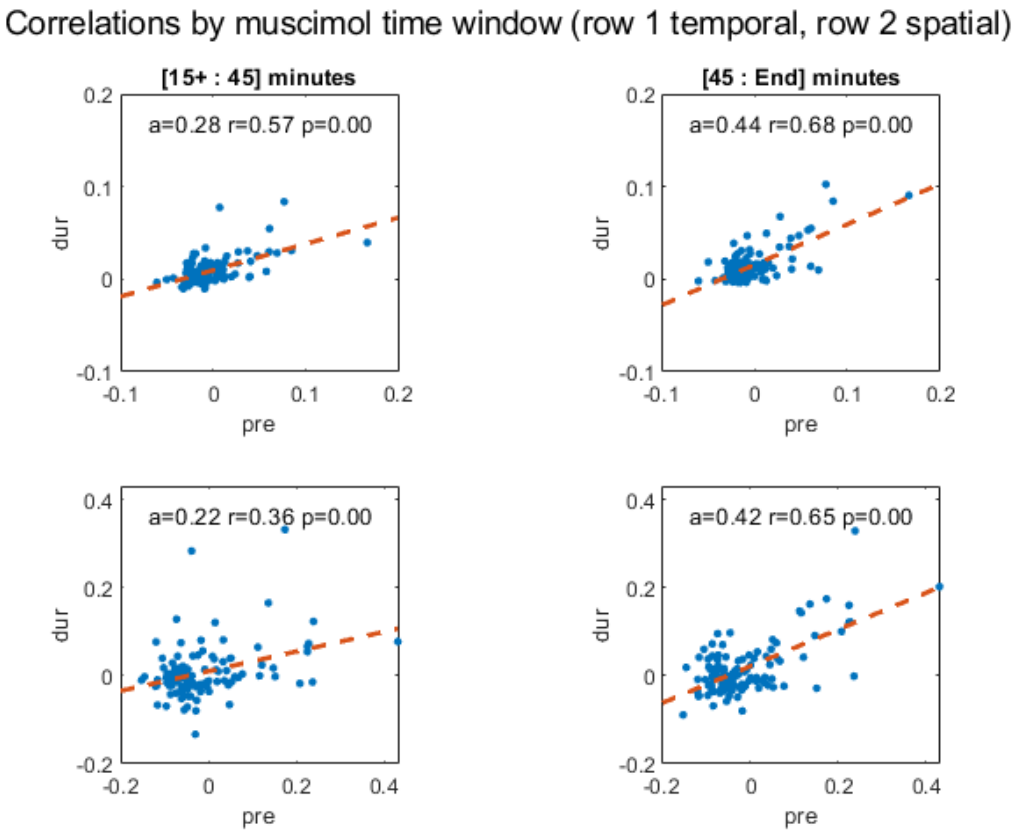

Figure 3 figure supplement 1. Temporal correlations pre-inactivation plotted against the recording period during inactivation used in this analysis for cell pairs in cohort; all recordings after muscimol injections are from 15 to 45 minutes (top left) and all remaining recordings are from 45 minutes (top right) of the muscimol recording session. Slope of the regression line (a), correlation coefficient (r) and p-value (p) are shown. The second row depicts the same plots for spatial correlations. Because recordings had different starting and ending times, [15+, end] are used to signify the start and end of the recording time; on average, recordings started 16 minutes after and ended 115 minutes after muscimol injection into the hippocampus.

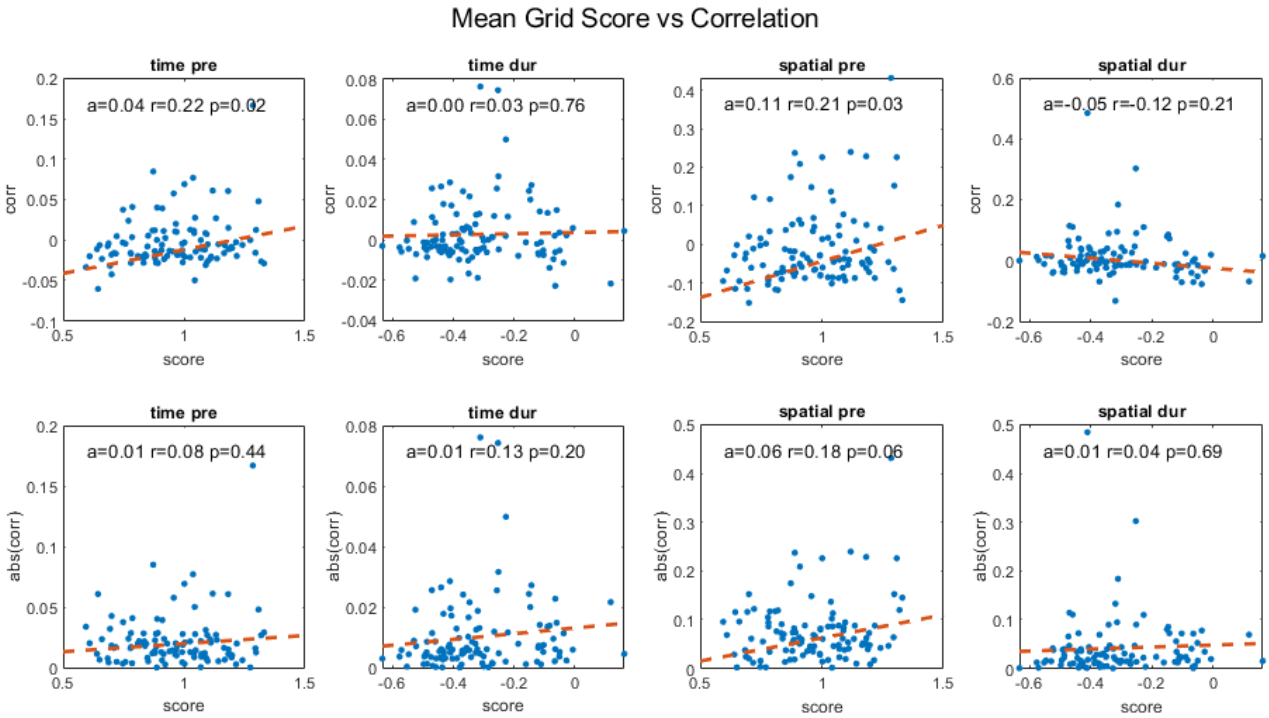

Figure 3 figure supplement 2 Temporal and spatial correlations for cell pairs in cohort pre- and during inactivation plotted against their average grid score, including slope of the regression line (a) correlation coefficient (r) and p-value (p). The second row shows the same plots for absolute correlation values.

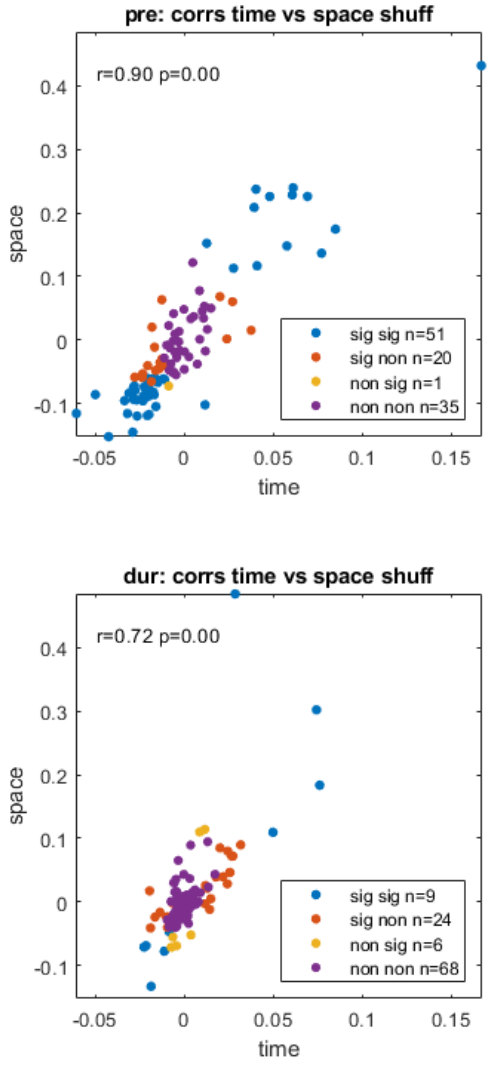

Figure 3 figure supplement 3. Temporal correlations plotted against spatial correlations for the cell pairs in our cohort, highlighted by significance, pre- (top) and during inactivation (bottom) with correlation coefficient (r) and p-value (p). The legend shows temporal significance followed by spatial significance, with either being significant (sig) or non-significant (non), i.e. 'non sig' implies the temporal correlation was non-significant and the spatial correlation was significant.

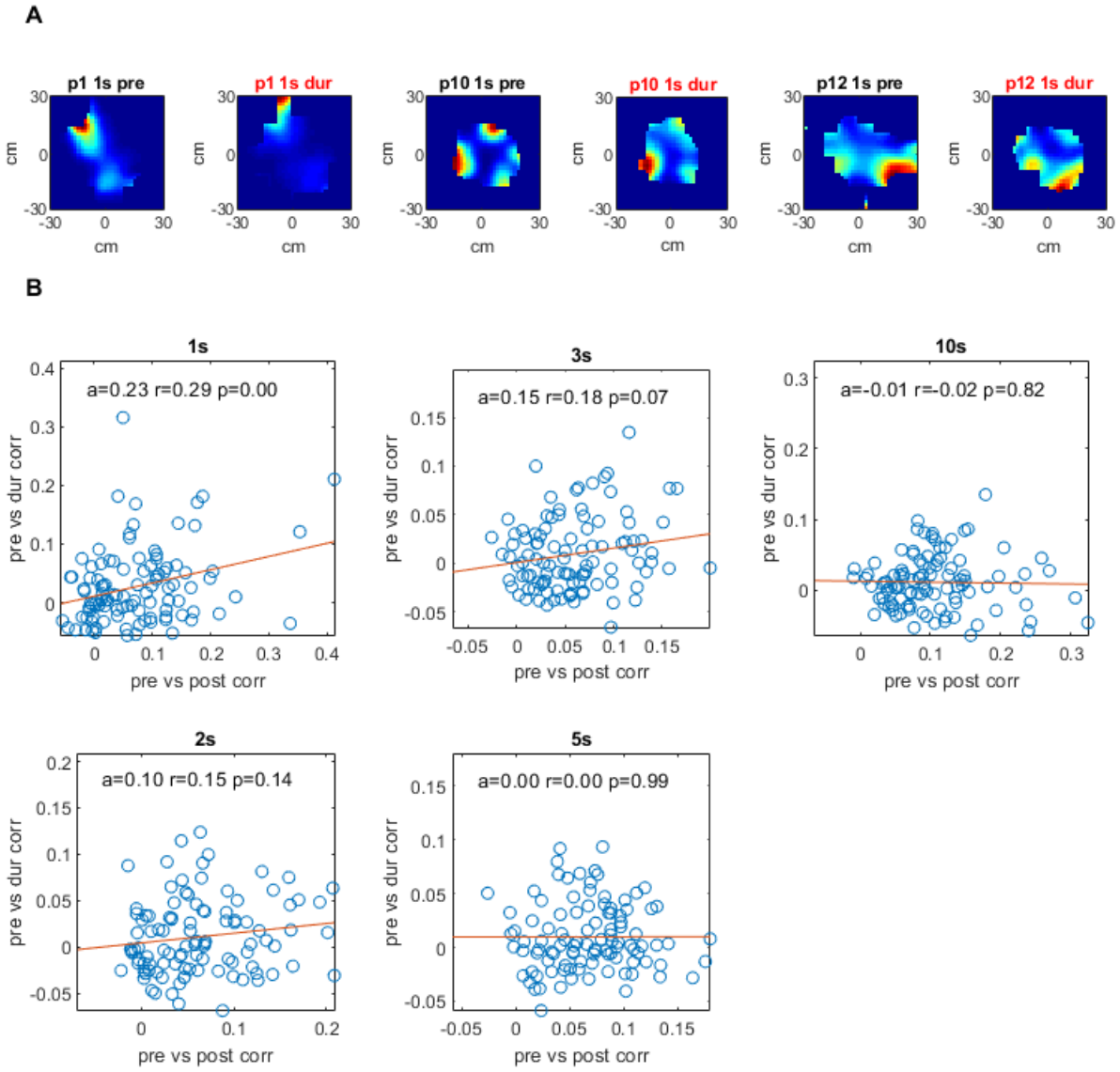

Figure 3 figure supplement 4 Drift rate plots for different time windows for all pairs in cohort. For each pair of cells: each spike's location was subtracted from that of all spikes from the second cell for a given time (t) window [-t, t]. These location differences were added to matrix of bins where the index [i,j] was the difference in cm for the spikes' x and y locations. This matrix was divided element-wise by a matrix of homologous construction where each bin represented the amount of time the animal spent for that x,y difference with respect to each spike, thus producing an aggregate rate matrix per cell pair. These 2D difference rate matrices are shown in (A) for a one second time window pre and during inactivation for three cell pairs. (B) shows these 2D matrices correlated to each other, pre vs during on the y axis, and pre vs post along the x axis, with slope of trendline (a), correlation coefficient (r) and p-value (p). For a more thorough description of this analysis see methods.

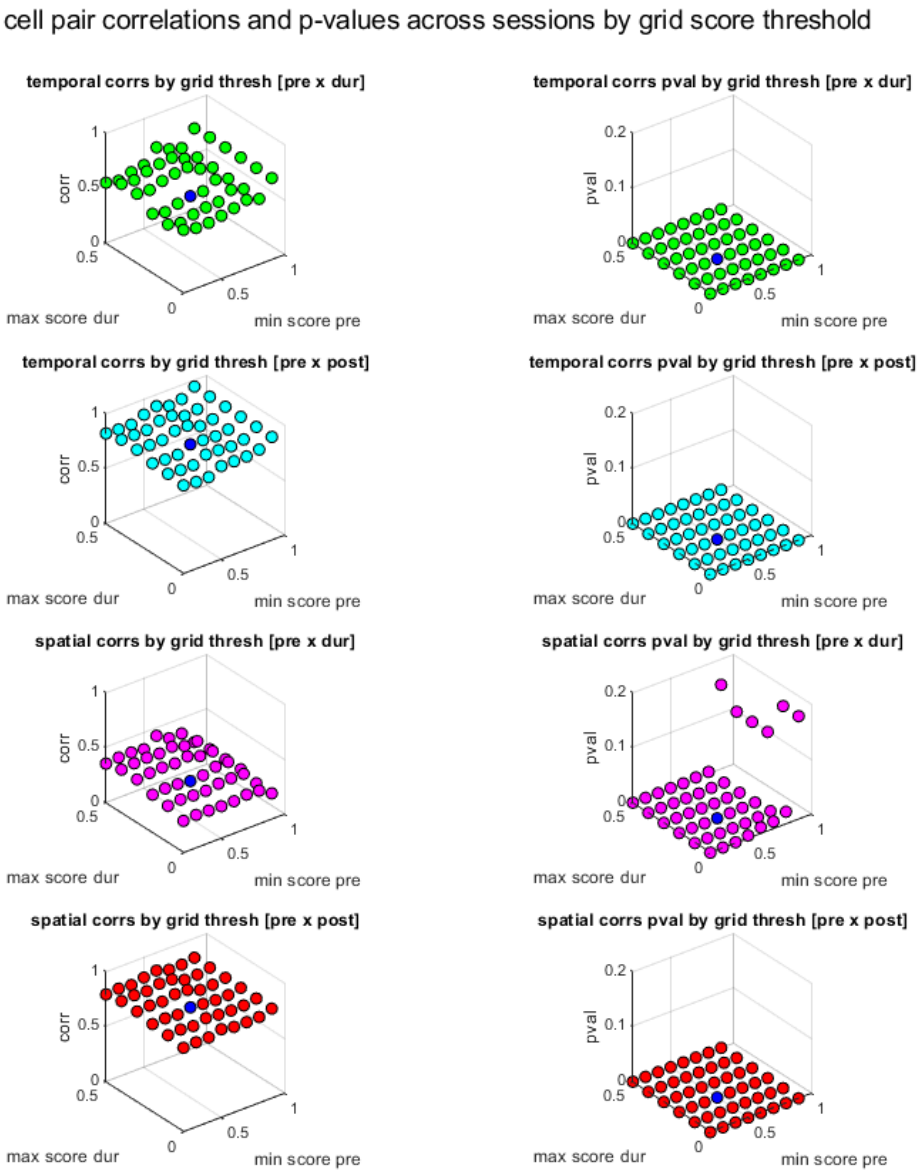

Figure 3 figure supplement 5. Cell pair correlations between sessions and p-values as a function of the grid score thresholds used in cell pair selections. In the first column, x and y axis show the pre and during inactivation grid score thresholds used to select simultaneously recorded cell pairs, the z axis shows the vector of those cell pair correlations (temporal and spatial) correlated against the same set of pairs for a different session (pre vs dur and pre vs post). The column on the right shows the corresponding p-value for each of those correlations. Note that blue is the actual value of thresholds used in the paper.

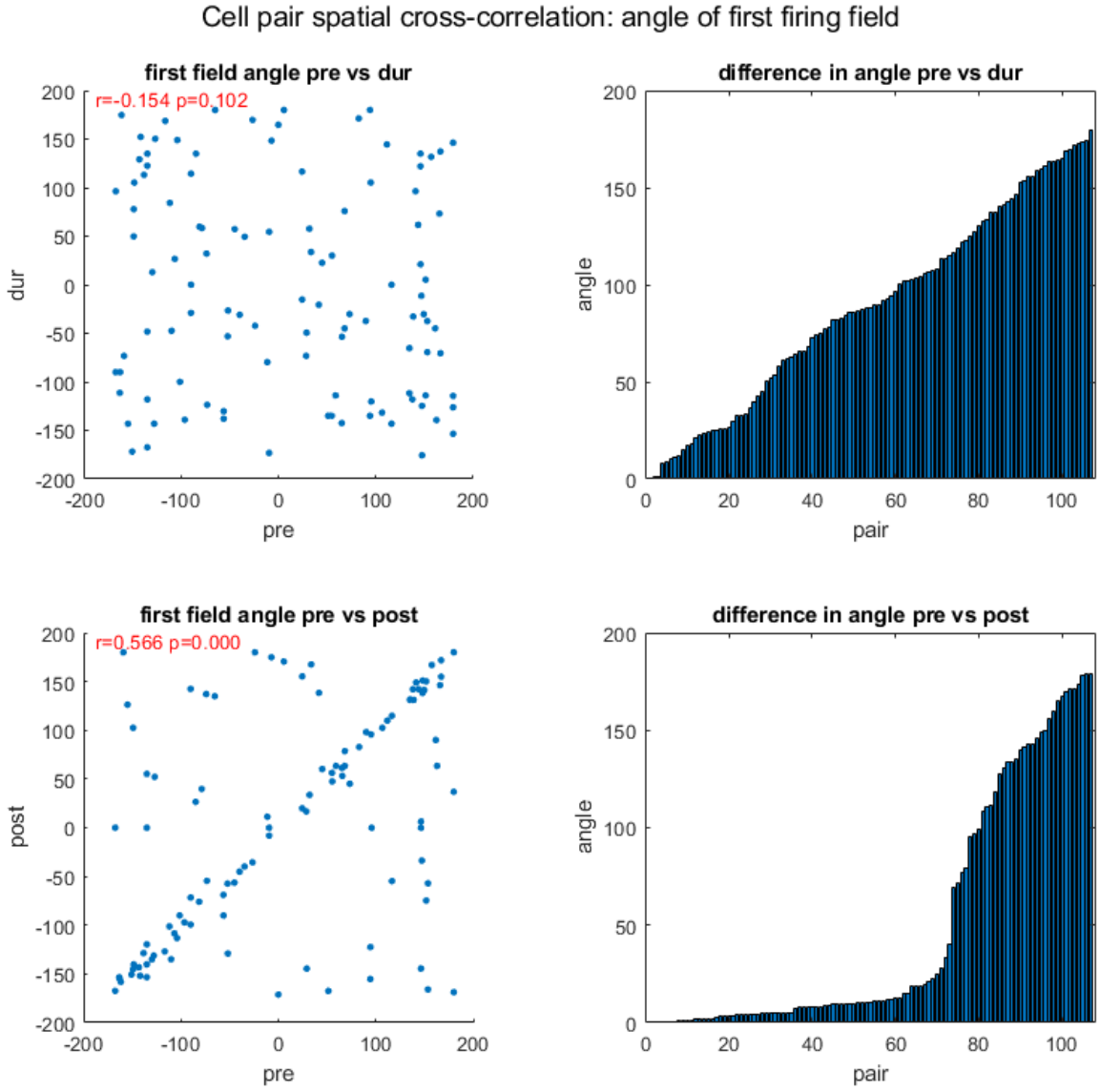

Figure 3 figure supplement 6. Examining the angle of firing fields for cross-correlated cells. Here the spatial firing rate maps of two sells are spatially cross correlated and the angle between the closest firing field to the center-most firing field is calculated. The first column shows scatter plots of the angle pre and during inactivation, and pre and post activation, including correlation using circular statistics (r) and corresponding p-value (p). The second column shows the difference in angle between two sessions for each cell pair, pre vs during, and pre vs post, y axis shows the angle difference, x axis the pair number (note the difference angles are sorted in ascending order, consequently the x axis only represents the pair number with respect to its own plot, not both). All angles are in degrees.

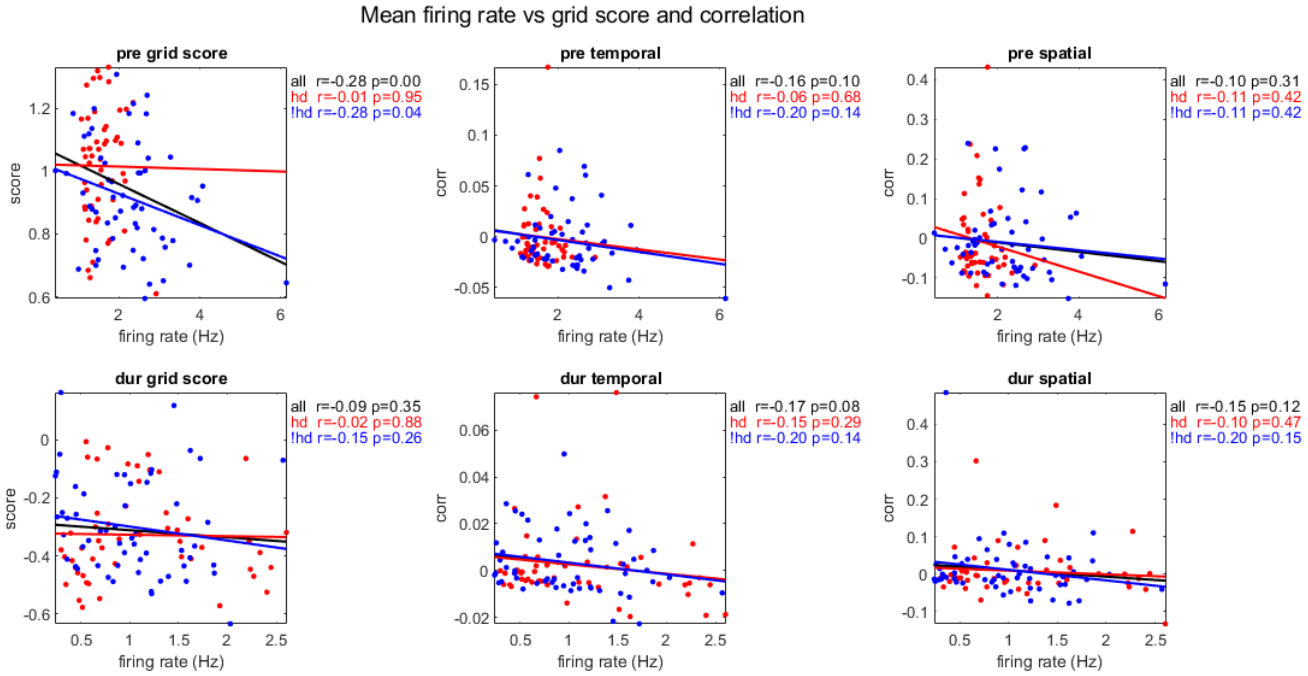

Figure 4 figure supplement 1. The mean firing rate of cohort cell pairs plotted against their mean grid score, temporal and spatial correlations, pre- and during inactivation (rows 1 and 2, respectively), grouped by cells with head directionality during inactivation (Rayleigh Score < 0.4 pre and > 0.4 during inactivation, red), without (Rayleigh Score < 0.4 pre during inactivation, blue), and all pairs in cohort (black), with correlation coefficient (r) and p-value (p).

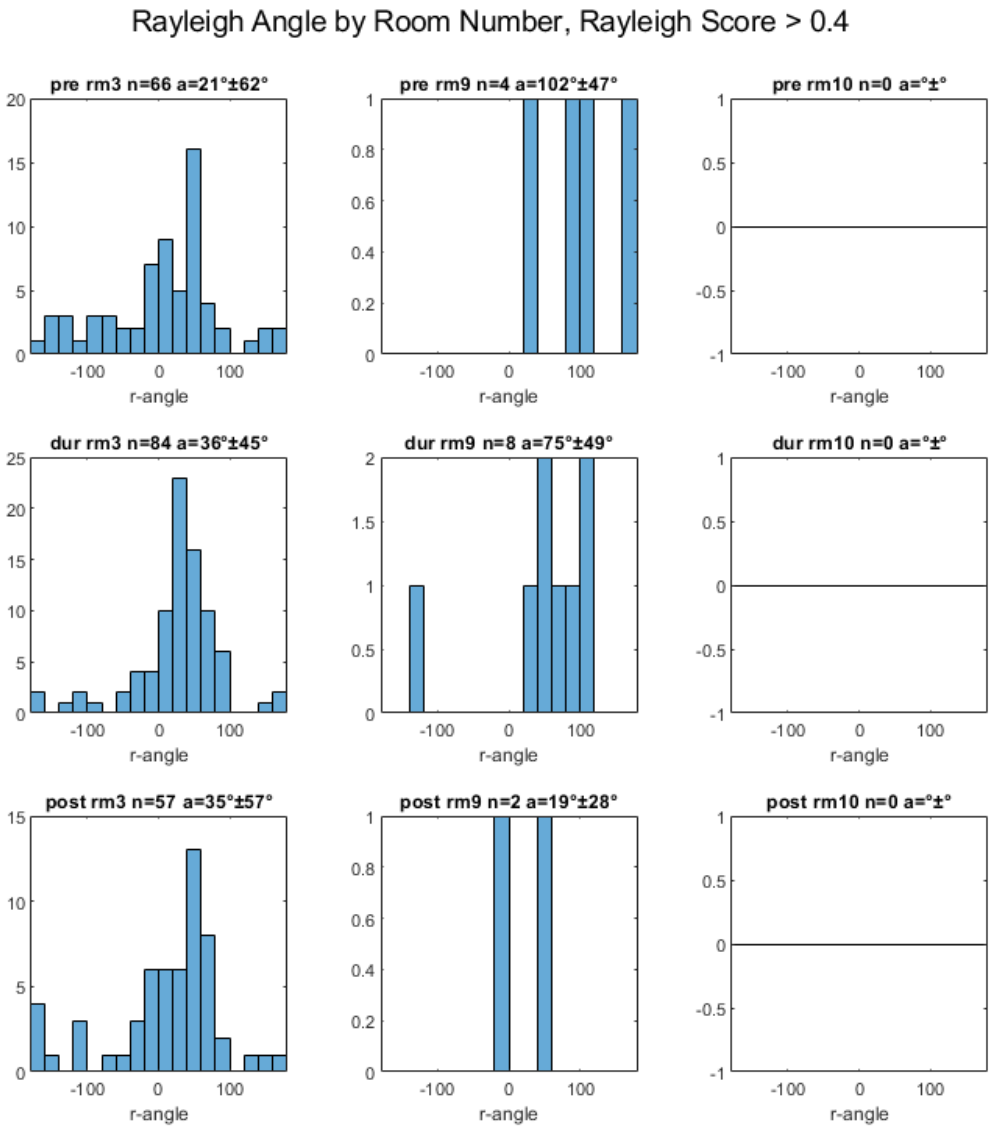

Figure 4, figure supplement 2 Rayleigh Angles for all head-direction cells in population by room number (rm#), for cells with Rayleigh Score greater than 0.4, pre-, during and post- inactivation (rows 1, 2, 3, respectively), with number of cells (n) and average (a) +- standard deviation angle. Note that most head-direction cells were recorded in room 3, and no head-direction cells were recorded in room 10.